Table 1
Characteristics of patients.

Case	Age/sex	Location	Histopathological diagnosis	Previous treatment	Symptoms
1	41/M	Cervical lymph node	SqCC	S, CH, Ra	ED, Pa
2	32/M	Cervical lymph node	Melanoma	S, CH	
3	82/F	Upper lip	AC	Th	ED, Pa
4	57/M	Maxilla	SqCC	S, CH, Ra	ED, Pa
5	67/F	Maxilla	MC	S, CH, Ra	ED, Pa, B
6	69/F	Maxilla	AC	S, CH, Ra	ED, Pa

SqCC: squamous cell carcinoma; AC: adenocarcinoma; MC: mucoepidermoid carcinoma; S: surgery; CH: chemotherapy; Ra: conventional radiotherapy; Th: thermotherapy; ED: eating disorder; Pa: pain; B: bleeding.

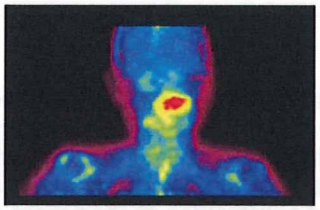

Fig. 1. ^{18}F-BPA-PET examination can visualize the distribution of boronophenylalanine (BPA).

used for measurement was removed at 10 min after the start of irradiation to evaluate epithermal neutron flux on a collimator Bi surface at a point 25 cm from the center and at the center of the irradiation field on the affected surface. The full-time exposure dose on the surface adjacent to the affected portion was determined by measuring neutron fluence (nvt) using gold and manganese wires. The absorbed dose of gamma rays was measured using a TLD (BeO), with the gold wire and TLD set in the vicinity of the center of the affected surface. The ^{10}B concentration in blood was determined by collecting venous samples every 30 min after BPA administration until just before irradiation, as well as after irradiation for prompt gamma radiation measurement.

Following BNCT, the tumor regression, adverse side effects, survival time, and subjective symptoms were recorded. For evaluating adverse side effects, the Common Terminology Criteria for Adverse Events v3.0 (CTCAE v3.0) was used. Tumor regression was evaluated by CT and MR imaging.

4. Results

T/N ratios calculated on the basis of the ^{18}F-BPA-PET results ranged from 1.9 to 4.0. The maximum dose to the tumor (Gy-Eq) was 20.1–39.1 Gy-Eq and the minimum 9.12–31.9 Gy-Eq, while the dose to the oral mucosa was 9.03–15.7 Gy-Eq and to the skin was 2.81–7.64 Gy-Eq (Table 2).

Tumor reduction was rated as PR in 4 cases, while 1 case was CR and 1 was PD. Notably, in Case 2 with metastasis to the lymph nodes that was within the BNCT irradiation range, the reduction was rated as CR (Fig. 2).

As for clinical improvement, pain was alleviated in all 5 cases in which pain was observed before the study and difficulty eating was improved in each of those. Especially in Cases 1 and 4, the patients, who were forced to stay in the hospital due to pain and difficulty eating, were temporarily discharged after BNCT. In Case 5, bleeding from the tumor was reduced. For adverse side effects, mucositis, fatigue, alopecia, impaired taste, and pharyngeal edema were observed, although none was severe. Neither myelosuppression nor osteomyelitis of the jaw bone was observed.

Three of the 6 patients survived for a range of 23–29 months after the final BNCT. In Case 1, a tumor in the cervical lymph node was markedly reduced after BNCT, then later became enlarged, which led to death from aspiration pneumonia 4 months later. In Case 2, a tumor in the cervical lymph node was reduced to the level of CR and the patient died from lung metastasis 16 months later. In Case 4, the tumor enlarged after therapy and the patient died 13 months later. The other 3 patients were alive at the time of writing (Table 3).

5. Discussion

^{10}B, a stable isotope of boron that captures a low-energy neutron, splits off into alpha-particles and Li atomic nuclei. Their ranges are approximately 9 and 4 μ, respectively, which are equivalent to the size of a tumor cell. BNCT makes use of the reaction and selectively destroys tumor cells by causing low-energy neutrons to react with ^{10}B preliminarily uptaken by tumor cells. The therapy was performed for the first time by Farr et al. (1954) for glioblastoma multiforme, after which Kato et al. (2004) began to utilize it for head and neck cancer that had relapsed after initial treatment, and reported 11 cases.

Oral cancer in the early stage of T1 or T2 is frequently treated with surgery. However, it is difficult to obtain a radical cure for progressive or recurrent cancer after completion of the initial treatment, even if multimodal approaches such as surgery, radiotherapy, and chemotherapy are used. Accordingly, improvements in therapeutic performance are not encouraging, unless some new therapeutic strategies are developed. We have been performing BNCT treatment for recurrent cancer that relapsed after completion of initial treatment, including surgery, chemotherapy, conventional radiation therapy, and thermotherapy since 2005.

In BNCT, tumor cells take up boron and then are selectively destroyed. This reduces the impact on normal cells, and adverse effects can be alleviated. In the 6 cases described in this report, myelosuppression and skin lesions, normally seen with conventional radiation therapy, were not observed. Notably, osteomyelitis of the maxillary bone, which often develops after conventional radiation therapy for oral cancer, was not seen. These findings are extremely significant clinically, as osteomyelitis of the jaw bone after radiation therapy can induce infection and fracture, which causes difficulty in dealing with the intense pain. In addition, the mucositis and fatigue observed in most cases were mild and rated as grade 2 or lower.

As for clinical response, 4 cases were rated as PR, with 1 case each as PD and CR. Case 2 is quite interesting. In this patient, BNCT was performed for metastasis to the cervical lymph nodes after initial surgery and chemotherapy for melanoma in the maxillary gingiva. With melanoma, the presence of metastasis to the lymph nodes affects the prognosis, as the 5-year survival rate is 39% for

Table 2
Parameters of BNCT.

Case	Boron compound	T/N ratio of ^{18}F-BPA	Dose (Gy-Eq)			
			Skin surface	Oral mucosa	Tumor peak	Tumor minimum
1	1BPA	4.0	4.93	14.4	39.1	15.0
	2BPA		2.85	9.52	25.5	10.3
2	1BPA	1.9	4.6	14.4	20.1	15.7
	2BPA+BSH		7.64	15.7	35.5	29.0
3	1BPA	3.2	4.1	15.4	34.6	31.9
	BPA		3.59	12.9	28.8	27.9
4	1BPA	3.4	3.22	9.13	21.6	9.12
	BPA		2.81	9.03	21.1	20.4
5	1BPA	2.2	3.74	15.3	24.8	22.0
6	1BPA	2.4	7.2	15.0	38.3	17.1

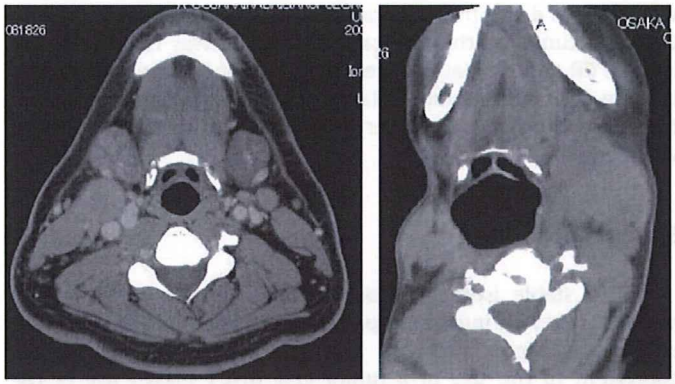

Fig. 2. Case2: Left: CT image taken before BNCT. Right: CT image taken after BNCT. Metastasis of the lymph node reduced completely.

Table 3
Clinical results.

Case	Clinical response I	Clinical response II	Adverse side effects (grade)	Outcome (duration after BNCT)
1	PD	DP, IE	M (2), F (1)	Died (4 months)
2	CR		M (3), F (1), AL (1), I (1), PE (2)	Died (16 months)
3	PR	DP, IE	M (2), F (1)	AD
4	PR	DP, IE	M (1), F (1)	Died (13 months)
5	PR	DP, IE, DB	M (1), AL (1)	AD
6	PR	DP, IE	M (2), F (1)	AD

DP: decreased pain; IE: improved eating; DB: decreased bleeding; M: Mucositis; F: fatigue; AL: alopecia; I: impaired taste; PE: pharyngeal edema; AD: alive with disease.

cases with metastasis to the lymph nodes, whereas it is 80% for negative cases (Goldsmith, 1970). Our patient died from lung metastasis at 16 months after BNCT. However, the metastasis had completely disappeared from the cervical lymph nodes where BNCT was administered, suggesting the effectiveness of BNCT for highly malignant melanoma.

The mouth has a variety of functions such as eating and talking, as well as aesthetic qualities. These functions are disturbed easily as oral cancer progresses, while QOL is severely affected when pain is added. BNCT is effective not only for reducing the size of the tumor, but also in controlling pain and decreasing bleeding, thus contributing to QOL improvement. The most important goal of this therapy is tumor regression, with complete cure and reintegration of the patient into normal life. However, this has yet to be achieved.

The success or failure of BNCT is dependent on whether the ^{10}B compound can be selectively taken up by the nuclei of the tumor cells. Miyatake et al. (2005) reported that the combination of BPA and BSH increased the ^{10}B concentration in patients with malignant brain tumors. In Case 2, we aimed at the cervical lymph nodes as the target and used BPA as the boron compound during the first irradiation. However, since the tumor peak dose was low at 20.1 Gy-Eq, we used BHS concomitantly during the second irradiation. As a result, the tumor peak dose elevated to 35.5 Gy-Eq and the target lymph nodes attained CR.

Although the number of cases presented was small, all of our cases were patients with recurrent or metastatic cancer after the completion of an initial treatment we considered that these patients might face difficulties not only with the therapeutic effect on the tumors, but also QOL improvement, if treated by conventional treatment. Although BNCT could not bring about a complete cure, it greatly improved the QOL of each patient without causing serious adverse side effects. For BNCT for the oral and maxillofacial region, additional detailed studies are necessary in regard to the method of fixing and positioning the patient. In a future study, we intend to investigate the detailed clinical and basic requirements to develop a more effective treatment method.

References

Coderre, J.A., Morris, G.M., 1999. The radiation biology of boron neutron capture therapy. Radiat. Res. 151, 1–18.

Farr, L.E., Sweet, W.H., Robertson, J.S., et al., 1954. Neutron capture therapy with boron in the treatment of glioblastoma multiforme. Am. J. Roentogenol. 71, 279.

Goldsmith, H.S., 1970. Prognostic significance of lymphnode dissection in the treatment of malignant melanoma. Cancer 26, 606–609.

Imahori, Y., Ueda, S., Omori, Y., et al., 1998. Fluorine-18-labeled fluoroboronphenylalanine PET in patients with glioma. J. Nucl. Med. 39, 325–333.

Kato, I., Ono, K., Sakurai, Y., et al., 2004. Effectiveness of BNCT for recurrent head and neck malignancies. Appl. Radiat. Isot. 61 (5), 1069–1073.

Miyatake, S., Kawabata, S., Kajimoto, Y., et al., 2005. Modified boron neutron capture therapy for malignant gliomas performed using epithermal neutron and two boron compounds with different accumulation mechanisms. J. Neurosurg., 1000–1009.

Applied Radiation and Isotopes 67 (2009) S109–S110

Contents lists available at ScienceDirect

Applied Radiation and Isotopes

journal homepage: www.elsevier.com/locate/apradiso

Disposition of TF-PEG-Liposome-BSH in tumor-bearing mice

Y. Ito [a,*], Y. Kimura [a], T. Shimahara [a], Y. Ariyoshi [a], M. Shimahara [a], S. Miyatake [b], S. Kawabata [b], S. Kasaoka [c], K. Ono [d]

[a] Department of Dentistry and Oral Surgery, Division of Medicine for Function and Morphology of Sensory Organs, Osaka Medical College, Japan
[b] Department of Neurosurgery, Osaka Medical College, Japan
[c] Faculty of Pharmaceutical Sciences, Hiroshima-International University, Japan
[d] Particle Radiation Oncology Research Center, Research Reactor Institute, Kyoto University, Japan

ARTICLE INFO

Keywords:
Boron neutron capture therapy (BNCT)
Mice
Oral SCC
BSH
Transferrin
Polyethylene-glycol
Liposome

ABSTRACT

BNCT requires high concentration and selective delivery of ^{10}B to the tumor cell. To improve the drug delivery in BNCT, we conducted a study by devising TPLB. We administrated three types of boron delivery systems: BSH, PLB and TPLB, to Oral SCC bearing mice. Results confirmed that ^{10}B concentration is higher in the TPLB group than in the BSH group and that TPLB is significantly effective as boron delivery system.

1. Introduction

To improve the efficacy of boron neutron capture therapy (BNCT) in the treatment of oral malignant tumors, a high concentration of boron uptake is required at the tumor cells. Furthermore, in order to minimize damage to normal cells, it is important that boron specifically concentrates and is retained for a long period of time in the tumor cells, while uptaking with a low concentration in normal cells (Barth et al., 1992). In other words, if boron can be retained only in the tumor cells for as long as possible during exposure, it is assumed that efficacy of BNCT can be improved. Consequently, a delivery system with a long retention time and high selectivity to the tumor cell is desired.

Although many delivery systems that can transport drug agents and can perform targeting have been studied, liposome was selected for this study as it shows high concentration in tumor cells, and can transport a large amount of boron macromolecules.

Since liposomes consist of a lipid membrane derived from a biomembrane, they do not have toxicity or immunogenicity and have excellent biocompatibility. Liposomes are also carriers which can encapsulate a large amount of drug agents without the mediation of chemical bonding (Gabizon and Papahadjopoulos, 1988).

In vivo, however, reticuloendothelial tissues, such as the liver, phagocytize the liposomes. As such, by modifying the liposome into a PEG-Liposome that can be retained in the blood, would reduce phagocytosis, and transport of boron to the tumor cells can be improved. Also, receptors which show high expression for the tumor cell are useful for the transport of the tumor-selective boron compound. Transferrin receptors are known to be over-expressed on the surface of cancer cells with respect to normal cells; by modifying the surface of PEG-Liposomes with transferrin (TF), the resulting liposomes (TF-PEG-Liposomes) targeted at these receptors may be considered to be an effective carrier as cancer targeting (Wagner et al., 1994).

In this study, Boron concentration at the oral squamous-cell carcinoma (SCC) cell in a cancer-bearing mice model was considered, using PEG-Liposome and TF-PEG-Liposome loaded with the boron compound sodium borocaptate (BSH).

2. Materials and methods

Cells, animals, and materials: SAS (from HSRRB) was used as the oral SCC cell line. A medium was mixed 1:1 with DMEM: F-12 medium, supplemented with 10% FBS and an antibiotic agent. SAS was cultured with the medium at 37°, 5% CO_2. PEG-Liposome-BSH (PLB), TF-PEG-Liposome-BSH (TPLB), (both provided by Dr. Kasaoka) (Doi et al., 2008), and BSH were used as boron compound.

Creation of cancer-bearing mice: SAS cells were collected after separating for trypsin EDTA, and then adjusted to 5×10^6 cells/0.1 mL. Five-week-old male BALB/c mice were anesthetized by inhalation anesthesia, and the adjusted SAS cells were injected under the dorsal skin.

* Corresponding author. Tel.: +81 726 83 1221; fax: +81 726 81 3723.
E-mail address: ora059@poh.osaka-med.ac.jp (Y. Ito).

0969-8043/$ - see front matter Crown Copyright © 2009 Published by Elsevier Ltd. All rights reserved.
doi:10.1016/j.apradiso.2009.03.018

Boron compound administration and tissue removal: Experiments were conducted when tumor cell mass diameter on the skin of the cancer-bearing mice reached 1 cm. After anesthetizing by inhalation anesthesia, various adjusted boron compounds at 35 mg^{10}B/kg (35 μg^{10}B/g) were administered to the cancer-bearing mice. The mice were then euthanized with an overdose of anesthesia 24, 48, and 72 h after administration. Physiological saline was allowed to flow back from the aorta, and then the tumor site, liver, and blood were removed. The removed tissue weight was measured, dissolved in nitric acid, and the sample solutions were used for ICP measuring.

Boron concentration measurement: ICP emission spectrometry using an ICP-AES P-5200 (HITACHI) was performed to measure boron concentration. The analytical curve derived from the boron standard solution with a measurement wavelength of 249.773 nm was used to measure the concentration. Luminescence intensity of the created sample solution was measured by ICP-AES. Boron concentrations of the solutions were measured according to the analytical curve, and the amount of boron was calculated as the boron concentration per weight of the tissue.

This study was based on the national regulations and guidelines, all experimental procedures were reviewed by the review committee for animal experiments of Osaka Medical College.

3. Results and discussion

The boron concentrations of BSH group were a low value at which tissues (blood, liver and tumor) and times (24, 48 and 72 h). The boron concentration of blood using PLB is blood–PLB group and using TPLB is blood–TPLB group. Blood–PLB group and blood–TPLB group were high in 24 h after administration, and both groups were decreased in 72 h. The boron values in 72 h of blood–PLB and blood–TPLB groups were about the same as BSH group. The boron concentration of liver using PLB is liver–PLB group and using TPLB is liver–TPLB group. The boron value was similar in the liver–PLB group and the liver–TPLB group. Both were high in 24 h, and decreased a little in 72 h. The boron concentration of tumor using PLB is tumor–PLB group and using TPLB is tumor–TPLB group. Tumor-PLB group was no difference in 24 and 48 h, but decreased in 72 h. However, tumor–TPLB group were no difference in 24, 48 and 72 h.

It seems that the TPLB has accumulated Boron in not only the tumor cell surroundings but also the tumor cells while the PLB accumulated Boron in the tumor cell surroundings. Therefore, it is thought that Boron remained accumulating in the tumor site for a long time (Maruyama et al., 2004).

4. Conclusions

This study showed a high concentration of TPLB to the oral SCC cells at the tumor site in vivo. Furthermore, high retention of TPLB in the blood could also be observed. In the future, the appropriate concentration and length of time to achieve BNCT efficacy, which will have a high concentration at the tumor site while not affecting surrounding tissues, could be estimated for SAS cells by measuring the change in boron concentration in various organs over time.

References

Barth, R.F., Soloway, A.H., Fairchild, R.G., Brugger, R.M., 1992. Boron neutron capture therapy for cancer. Realities and prospects. Cancer 70, 2995–3007.

Doi, A., Kawabata, S., Iida, K., Yokoyama, K., Kajimoto, Y., Kuroiwa, T., Shirakawa, T., Kirihata, M., Kasaoka, S., Maruyama, K., Kumada, H., Sakurai, Y., Masunaga, S., Ono, K., Miyatake, S., 2008. Tumor-specific targeting of sodium borocaptate (BSH) to malignant glioma by transferrin-PEG liposomes: a modality for boron neutron capture therapy. J. Neurooncol. 87, 287–294.

Gabizon, A., Papahadjopoulos, D., 1988. liposome formulations with prolonged circulation time in blood and enhanced uptake by tumors. Proc. Natl. Acad. Sci. USA 85, 6949–6953.

Maruyama, K., Ishida, O., Kasaoka, S., Takizawa, T., Utoguchi, N., Shinohara, M., Chiba, M., Kobayashi, H., Eriguchi, M., Yanagie, H., 2004. Intracellular targeting of sodium mercaptoundecahydrododecaborate (BSH) to solid tumors by transferrin-PEG liposomes, for boron neutron-capture therapy (BNCT). J. Controlled Release 98, 195–207.

Wagner, E., Curiel, D., Cotton, M., 1994. Delivery of drugs, proteins and genes into cells using transferrin as a ligand for receptor-mediated endocytosis. Adv. Drug Delivery Rev. 14, 113–135.

Biomaterials 31 (2010) 4139–4145

Contents lists available at ScienceDirect

Biomaterials

journal homepage: www.elsevier.com/locate/biomaterials

Development of a bifunctional immunoliposome system for combined drug delivery and imaging *in vivo*

Bin Feng [a,d], Kazuhito Tomizawa [b,*], Hiroyuki Michiue [a], Xiao-Jian Han [a], Shin-ichi Miyatake [c], Hideki Matsui [a]

[a] Department of Physiology, Okayama University Graduate School of Medicine, Dentistry and Pharmaceutical Sciences, 2-5-1 Shikata-cho, Okayama 700-8558, Japan
[b] Department of Molecular Physiology, Faculty of Medical and Pharmaceutical Sciences, Kumamoto University, Kumamoto 860-8558, Japan
[c] Department of Neurosurgery, Osaka Medical College, 2-7 Daigaku-machi, Takatsuki Osaka 569-8686, Japan
[d] Department of Biotechnology, Dalian Medical University, Dalian 116044, China

ARTICLE INFO

Article history:
Received 16 October 2009
Accepted 15 January 2010
Available online 10 February 2010

Keywords:
Glioma cells
EGFR
Immunoliposome
Gaussia luciferase
Bioluminescence
Boron neutron capture therapy

ABSTRACT

The diverse characteristics of immunoliposomes provide advantages for utilization in drug delivery systems. In this study, we fused the antibody affinity motif of protein A (ZZ) with *Gaussia* luciferase (GLase). The fused protein conjugated with an anti-epidermal growth factor receptor (EGFR) monoclonal antibody (GLase-ZZ-His-mAb) was effectively delivered into glioma cells expressing an activated EGFR mutant (EGFRvIII) and the bioluminescence was visualized in the cells. Immunoliposomes were further constructed with DSPE-PEG-MAL for covalent GLase-ZZ-His-mAb conjugation. A fluorescence dye (HPTS) encapsulated in immunoliposomes conjugated with GLase-ZZ-His-mAb was effectively delivered into EGFRvIII-expressing glioma cells. In a murine xenograft model of glioma, moreover, specific targeting of the immunoliposomes was visualized in the tumor. This new bifunctional immunoliposome system has the potential for drug delivery and imaging *in vivo*.

1. Introduction

Liposomes, comprised of naturally-occurring non-cytotoxic phospholipids and cholesterols, have been recognized as a potential drug delivery vehicle for three decades [1]. Their ability to encapsulate water-soluble compounds as well as non-toxic nature surpasses that of all other nanomaterial-based drug delivery platforms [2]. Also, by altering lipid composition, size and surface chemistry, liposomes can be developed into multifunctional constructs to meet the tunable requirements of different DDSs, such as combining diagnostic and therapeutic capabilities, thus providing a universal platform that can simultaneously detect, image and target diseased cells [2].

In recent years, targeted liposomes have emerged as viable candidates for tumor imaging and therapy [3,4]. Tumor-targeting ligands, such as antibodies, or receptor ligands such as folate [5], transferrin [6] and epidermal growth factor (EGF) [7], have been used for targeted ^{10}B delivery in boron neutron capture therapy (BNCT). Targeted liposomes provide an advantage over untargeted liposomes not only because of increased localization to tumor sites but also because of increased interaction with the target cell population once at the tumor sites [8]. Immunoliposomes have also been used to deliver contrast agents and radionuclides for diagnostic imaging and therapy [9–12]. Semiconductor quantum dots (QDs) conjugated to liposomes are used for imaging, and the immunoliposomes are successfully observed *in vitro* and *in vivo* [13].

For real-time imaging in small animals, the bioluminescence produced by the enzymatic reaction of a luciferase with a luciferin has been used to non-invasively monitor biological processes [14]. The methods based on a luciferase–luciferin reaction have been applied to the imaging of tumors in mice with firefly luciferase [15], *Renilla* luciferase [16], and *Vargula* luciferase [17]. As a coelenterazine-dependent luciferase, *Gaussia* luciferase (GLase) was cloned from a marine copepod *Gaussia princes* and has recently been validated as a reporter gene for *in vivo* imaging applications [18,19]. Its small size (19.9 kDa) and independence of ATP make it suitable for detecting bioluminescence when fused with another protein [20–22].

We previously used the antibody affinity motif of protein A (ZZ) as an adaptor to conjugate anti-EGFR antibodies to sodium borocaptate (BSH)-encapsulated nickel-liposomes. The formed immunoliposomes effectively and specifically delivered BSH into EGFR-overexpressing glioma cells *in vitro* and *in vivo* [23]. In the

* Corresponding author. Tel.: +81 96 373 5050; fax: +81 96 373 5052.
E-mail address: tomikt@kumamoto-u.ac.jp (K. Tomizawa).

0142-9612/$ – see front matter © 2010 Elsevier Ltd. All rights reserved.
doi:10.1016/j.biomaterials.2010.01.086

present study, ZZ fused with GLase was used not only as an adaptor to conjugate mAb, but also as an imaging component for detection. Two glioma cell lines, PA U87 not expressing EGFR, and U87 ΔEGFR-overexpressing human EGFR variant III (vIII), were employed to evaluate the efficiency with which the fluorescence dye was delivered and imaging was achieved using the immunoliposomes *in vitro* and *in vivo*.

2. Materials and methods

2.1. Lipids and chemicals

DSPE-PEG-MAL (maleimide), DSPE-PEG_{2000}, DOPC and DOPG were purchased from Nippon Oil and Fats (Tokyo, Japan). Cholesterol, chloroform and diethyl ether were acquired from Wako Pure Chemicals (Japan). 8-Hydroxypyrene-1,3,6-trisulfonic acid trisodium salt (HPTS) and Traut's Reagent (2-Iminothiolane.HCl) were purchased from Sigma–Aldrich and Coelenterazine was purchased from NanoLight Technology.

2.2. Cell lines

U87 ΔEGFR and PA U87 glioma cell lines (kindly donated by Professor Webster K. Cavenee of the University of California at San Diego) were used in all experiments. U87 ΔEGFR cells stably express the constitutively active EGFR, EGFRvIII, whereas PA U87 cells express no EGFR. The cells were maintained in Dulbecco's modified Eagle's medium (DMEM) (Invitrogen) with 10% fetal bovine serum (FBS), penicillin and streptomycin at 37 °C in a humidified atmosphere containing 5% CO_2.

2.3. Expression and purification of recombinant GLase-ZZ-His

The pGLuc plasmid was purchased from LUX biotechnology Ltd (Scotland, UK).The GLase gene was amplified from the plasmid using a sense primer (5′-GAGCTCCATGAAACCAACTGAAAACAATG-3′, underline indicates *Sac*I site) and antisense primer (5′-AAGCTTATCACCACCGGCACCCTT-3′, underline indicates *Hind*III site). The PCR product was ligated into the pCR2.1 TOPO vector (Invitrogen), and digested with *Sac*I and *Hind*III. The digested GLase fragment was then inserted between the *Sac*I-*Hind*III site in the ZZ-His expression plasmid [23]. The recombinant plasmid was transformed into *E. coli* BL21 (DE3). The expression and purification of GLase-ZZ-His were performed as described previously [24].

2.4. Conjugation of GLase-ZZ-His with anti-EGFR antibody or FITC

To conjugate GLase-ZZ-His with the anti-EGFR mouse antibody (101-7300-0, Katayama Chemical Inc., Japan), the two were mixed at a molar ratio of 100:1 (GLase-ZZ-His to antibody) in 200 μL of PBS (pH7.4) and rotated at 4 °C for 2 h to yield GLase-ZZ-His-mAb.

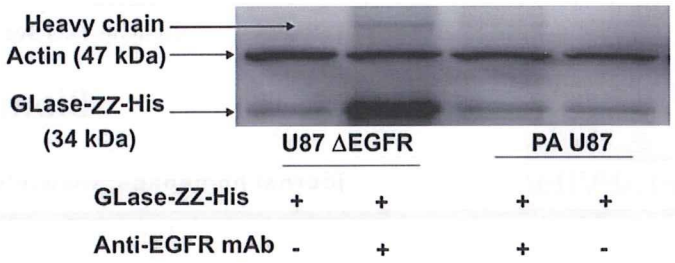

Fig. 1. Antibody-mediated delivery of GLase-ZZ-His into EGFR-overexpressing glioma cells. GLase-ZZ-His-mAb and GLase-ZZ-His were incubated with U87 ΔEGFR and PA U87 for 2 h. After a wash with PBS, cell lysate was subjected to 10% SDS-PAGE and transferred to PVDF membranes. The delivered proteins were detected by Western blotting using anti-His mouse mAb.

For the preparation of FITC-GLase-ZZ-His, GLase-ZZ-His was incubated with 1 mg/mL of fluorescein isothiocyanate isomer I (FITC, Sigma–Aldrich) at room temperature for 15 min with further incubation at 4 °C overnight in PBS as described [25]. The molar ratio of FITC to GLase-ZZ-His was 2:1. After incubation, non-reacted FITC was removed using a PD-10 column (Amersham). To conjugate FITC-GLase-ZZ-His with the anti-EGFR mouse antibody (FITC-GLase-ZZ-His-mAb), the two were mixed at the molar ratio mentioned above.

2.5. Confirmation of the delivery of GLase-ZZ-His-mAb and FITC-GLase-ZZ-His-mAb in cells

PA U87 and U87 ΔEGFR cells were incubated with 3 μM of GLase-ZZ-His-mAb. As a control, the cells were incubated with 3 μM of GLase-ZZ-His. After 2 h, the cells were washed with PBS twice and treated with 0.025% trypsin to remove surface-bound antibody. They were then resuspended in PBS twice before sonication and subjected to Western blotting using an anti-His mouse monoclonal antibody (C-term, Invitrogen). The Western blotting was carried out as described previously [26]. After incubation with the appropriate secondary antibody conjugated with horseradish peroxidase (Sigma–Aldrich), positive bands were visualized using an enhanced chemiluminescence detection system (Amersham Biosciences, Pittsburgh, PA).

After 3 h of incubation with FITC-GLase-ZZ-His-mAb, U87 ΔEGFR and PA U87 cells were washed with PBS twice, then fixed with 4% paraformaldehyde (PFA) for 10 min, and washed with PBS three more times. Fluorescence was observed using

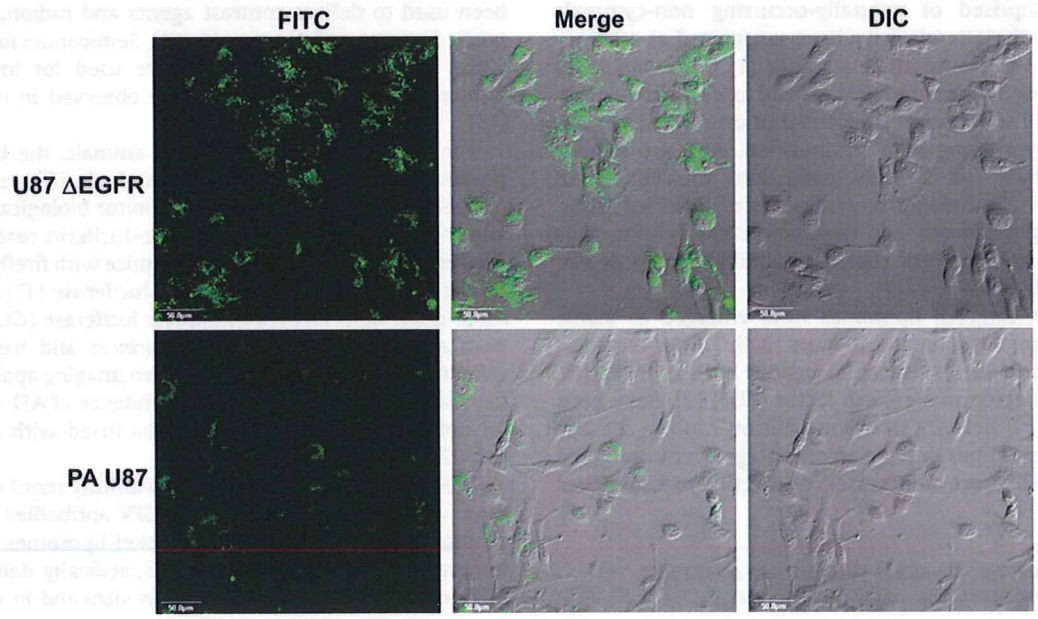

Fig. 2. Fluorescence-based detection of GLase-ZZ-His delivered by the antibody. U87 ΔEGFR and PA U87 cells were incubated with FITC-GLase-ZZ-His-mAb for 2 h and fixed with 4% PFA. Fluorescence was visualized using a confocal laser microscope. Bar = 50 μm.

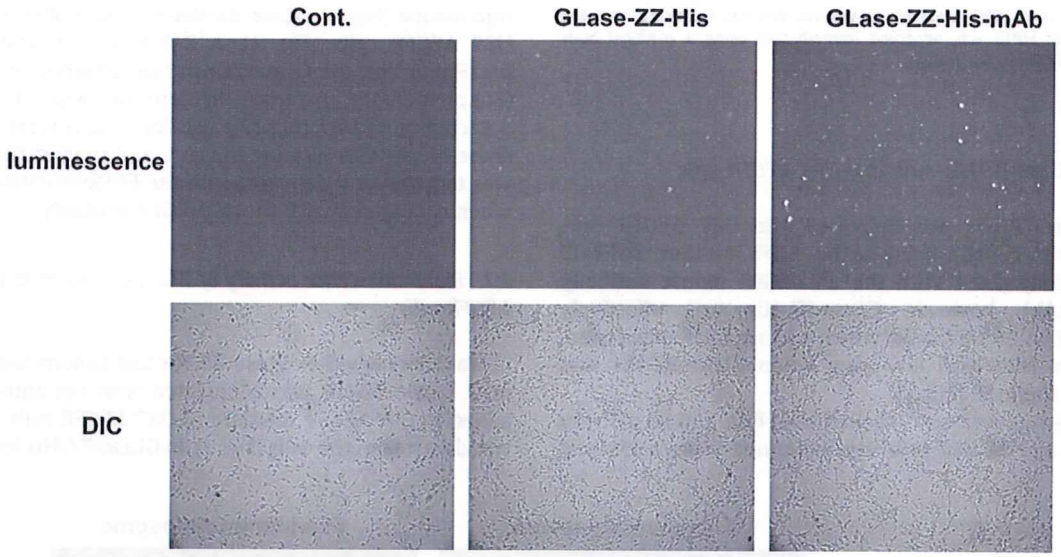

Fig. 3. Bioluminescence-based detection of GLase-ZZ-His in U87 ΔEGFR cells. U87 ΔEGFR cells were incubated with GLase-ZZ-His and GLase-ZZ-His-mAb for 2 h. After being washed with culture medium without serum, the cells were treated with coelenterazine and immediately observed under a bioluminescence microscope.

a confocal laser microscope (FluoView, Olympus, Japan). In the control, only FITC-GLase-ZZ-His was added.

2.6. Bioluminescence imaging of GLase-ZZ-His in cells

To detect the bioluminescence of GLase-ZZ-His, U87 ΔEGFR cells were cultured on a 35-mm glass-bottomed dish for 24–48 h. GLase-ZZ-His-mAb and GLase-ZZ-His were added at 3 μM and the cells were incubated for 2 h, washed with DMEM two times, and soaked with 1 mL of serum-free DMEM containing 1 μg/mL of coelenterazine. Luminescence was immediately recorded with an Olympus Luminoview LV 200 (Bioluminescence microscope (BLM)) after the addition of coelenterazine. Images were acquired and analyzed with Metamorph software (Molecular devices).

2.7. Construction of GLase-ZZ-His-immunoliposomes

Liposomes composed of DOPC: DOPG: CH: DSPE-PEG-MAL: DSPE-PEG$_{2000}$ (3:3:4:0.1:0.1, molar ratio) were prepared by lipid film hydration as described previously with a slight modification [27]. Briefly, 100 μmol of lipid dissolved in 2 mL of a chloroform/diethyl ether mixture (1:1 v/v) was added to a rotary evaporator to form a lipid film under reduced pressure. Two milliliters of PBS containing 35 mM HPTS was then added and the lipid film was vortexed. To control size and lamellarity, the suspension was sonicated by a tip-type ultrasonic homogenizer (output level 7, TAITEC ULTRS Homogenizer VP-5S, Tokyo, Japan) for 5 × 1 min with 1 min ice cooling interval between each round. Then the liposome emulsion was extruded 10 times through a polycarbonate membrane 100 nm in pore size using an extruder device at 50 °C. The mean diameter of the prepared liposomes was determined with an electrophoretic light scattering spectrophotometer (ELS-8000, Photal, Tokyo, Japan). Unencapsulated free HPTS was removed by a PD-10 desalting column (Amersham).

For protein thiolation, GLase-ZZ-His was incubated with Traut's reagent at a molar ratio of 1:2 in PBS (pH7.4) with 0.5 M EDTA. After incubation at room temperature for 1 h, the thiolated GLase-ZZ-His was separated using a PD-10 column, and the fractions containing thiolated GLase-ZZ-His were pooled. Under a nitrogen atmosphere, HPTS-loaded liposomes containing DSPE-PEG$_{2000}$-maleimide were incubated with thiolated GLase-ZZ-His (molar ratio of DSPE-PEG$_{2000}$-maleimide to GLase-ZZ-His, 40:1) overnight at room temperature at a low rotating speed [28]. Free GLase-ZZ-His was removed with a Sepharose CL-4B column (1 × 10 cm) and the eluted GLase-ZZ-His-liposomes (Hereafter abbreviate as pre-immunoliposomes) were concentrated and the protein concentration was measured with a Biadford protein assay (Bio-rad). For constructing the immunoliposomes conjugated with anti-EGFR mouse antibody (mAb), the antibody was mixed with pre-immunoliposomes at a molar ratio of 1:20 (mAb to GLase-ZZ-His) at 4 °C with rotation for 2 h. Free mAbs were removed with a Sepharose CL-4B column. The lipid in each fraction was analyzed by the DAOS method using a Phospholipids C reagent kit (Wako Pure Chemical Inc. Ltd., Japan)

2.8. Fluorescence signal and luciferase detection in immunoliposome-treated cells

U87 ΔEGFR cells were cultured on laminin (20 μg/mL)-coated 3 cm dishes (2 mL medium) for 24–48 h, after which immunoliposomes and pre-immunoliposomes were added. The final concentrations of liposome (total lipid), GLase-ZZ-His, and antibody were 1 mM, 2 μM, and 3 μg/mL, respectively. After 2 h incubation, the cells were washed with DMEM twice, fixed with 4% PFA for 10 min, and washed with PBS twice again. Fluorescence signals were observed using a confocal laser microscope. For the detection of GLase-ZZ-His in immunoliposome-treated cells, U87 ΔEGFR cells were washed with DMEM and bioluminescence signals were analyzed as mentioned in 2.6.

2.9. Bioluminescence imaging in vivo

U87 ΔEGFR cells (1 × 10^6 cells/100 μL) were implanted into the back of female 4-to-6 week-old nude mice (15–20 g, BALB/c Slc-nu/nu; Japan SLC). After 10–14 days, animals bearing palpable tumors were administered intravenously 400 μL of immunoliposomes and pre-immunoliposomes via the tail. After 4 h, mice were imaged by injecting 50 μL of coelenterazine solution (100 μg/mL) at the tumor site under anesthesia using a cooled CCD (IVIS, Xenogen, Alameda, CA) camera as described previously [22]. The intensity of the selected region over the tumor was recorded as maximum photons s^{-1} cm^{-2} steradian^{-1}. To obtain control signal intensity, same amount of coelenterazine was injected to the site without tumor.

2.10. Slice analysis for determining HPTS's distribution in tumor

The immunoliposome-injected mice were sacrificed soon after bioluminescence imaging and tissues containing the tumor were excised. Sections 10-μm thick were

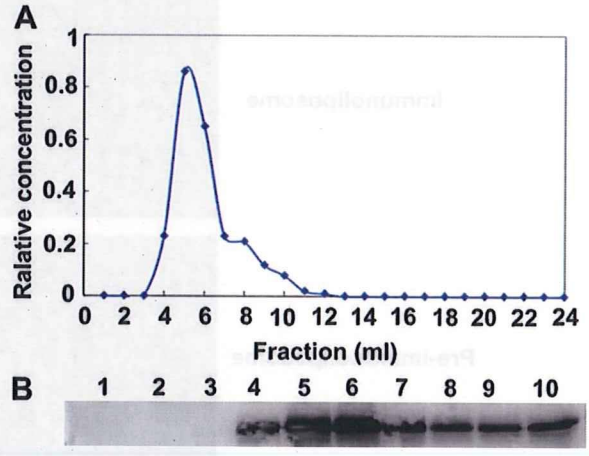

Fig. 4. Characterization of GLase-ZZ-His conjugated to liposomes. (A) GLase-ZZ-His-immunoliposomes (pre-immunoliposomes) were eluted through a Sepharose column and detected by lipid analysis. (B) Ten-microliter aliquots of eluted pre-immunoliposome samples were subjected to 10% SDS-PAGE and transferred to PVDF membranes. Anti-His mouse monoclonal antibody was used for the detection of GLase-ZZ-His.

cut on a microtome (CM 1850, Leica Microsystems, Wetzlar, Germany) and the fluorescence signal of HPTS was observed immediately using a confocal laser microscope (FluoView, Olympus, Japan).

3. Results

3.1. Delivery of GLase-ZZ-His-mAb into U87 ΔEGFR cells

Little of GLase-ZZ-His was delivered into U87 ΔEGFR cells overexpressing the constitutively active EGFR mutant, EGFRvIII (Fig. 1). When conjugated with the anti-EGFR mouse antibody (GLase-ZZ-His-mAb), however, GLase-ZZ-His was effectively delivered (Fig. 1). In PA U87 cells, which had no EGFR expression, the GLase-ZZ-His level was low even when GLase-ZZ-His was conjugated with the mAb (Fig. 1).

GLase-ZZ-His-mAb was next labelled with FITC and its delivery into U87 ΔEGFR and PA U87 cells was examined using a confocal microscope (Fig. 2). GLase-ZZ-His-mAb was observed in almost all U87 ΔEGFR cells (Fig. 2). A Z-dimensional scan excluded the possibility that the GLase-ZZ-His was attached to the cell surface (Supplementary material). In contrast, weak fluorescence was detected in PA U87 cells (Fig. 2). The results were consistent with those of Western blotting in Fig. 1, and suggest that GLase-ZZ-His was targeted and delivered into the EGFRvIII-overexpressing cells when conjugated with the anti-EGFR antibody.

3.2. Bioluminescence activity of GLase-ZZ-His-mAb in U87 ΔEGFR cells

To clarify whether GLase-ZZ-His had bioluminescence in glioma cells, GLase-ZZ-His was conjugated with the anti-EGFR mAb and added to the culture medium of U87 ΔEGFR cells. A strong signal was detected in the cells (Fig. 3). In GLase-ZZ-His incubated cells, in

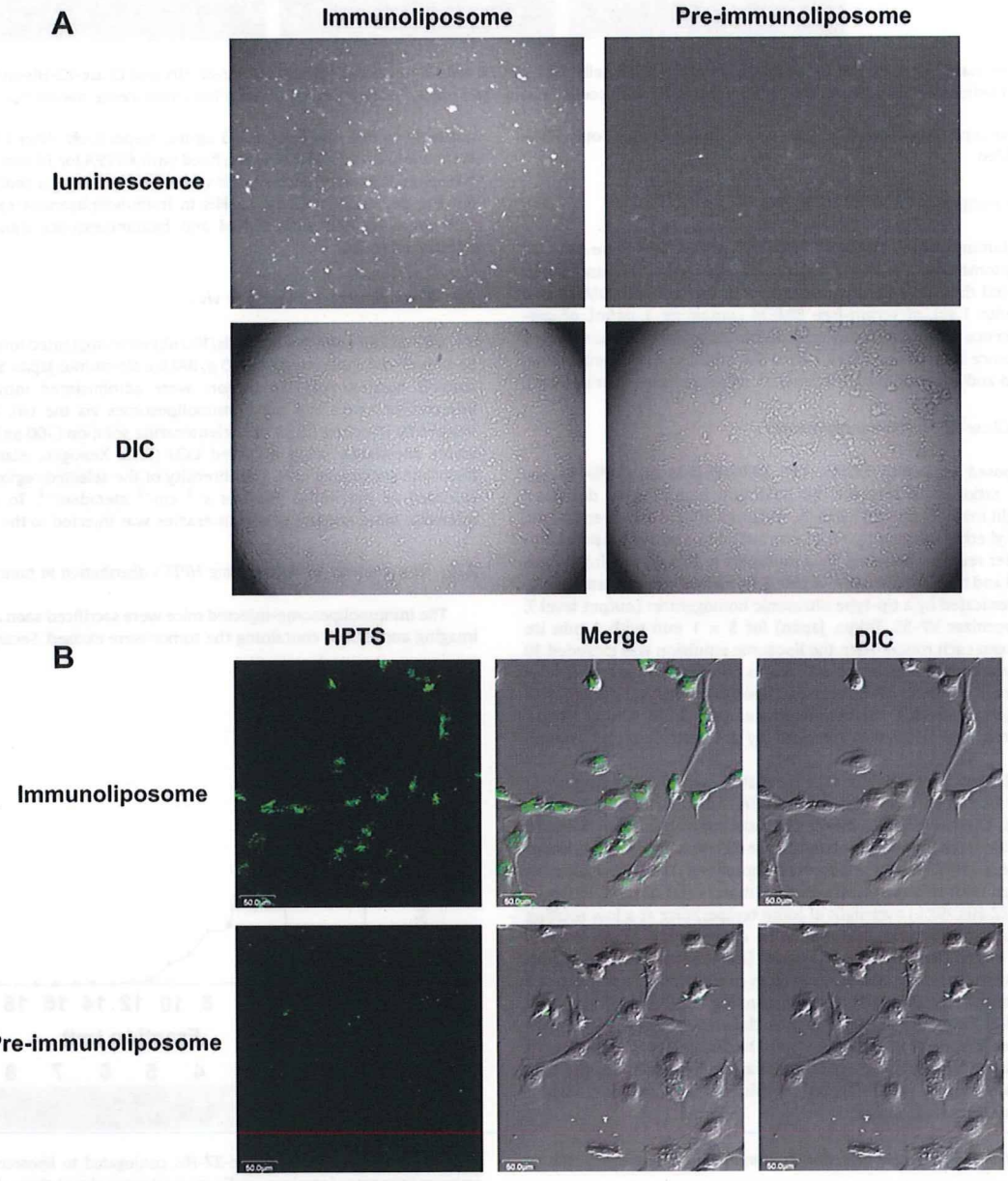

Fig. 5. Bioluminescence and fluorescence-based detection of immunoliposomes delivered into glioma cells. (A) U87 ΔEGFR cells were incubated with immunoliposomes and pre-immunoliposomes for 2 h. After a washing with DMEM, the luminescence was recorded soon after the coelenterazine substrate was added to cells. (B) After the luminescence was observed, the same samples were observed under a confocal microscope to detect fluorescence. Bar = 50 μm.

contrast, weak bioluminescence was detected in a few cells (Fig. 3). The bioluminescence was underdetectable in intact cells (Cont.). These results suggest that the fusion of ZZ-His with GLase did not affect its luciferase function.

3.3. Confirmation of the conjugation of GLase-ZZ-His with pre-immunoliposomes

To investigate whether thiolated GLase-ZZ-His effectively reacted with the maleimide (MAL) group on the liposome's surface, we compared the position of the GLase-ZZ-His and pre-immunoliposome after their separation with Sepharose CL-4B. The peak of the pre-immunoliposome occurred between fractions 5 and 6 (Fig. 4A). Western blotting revealed that GLase-ZZ-His was also abundant in these fractions (Fig. 4B). The results showed that thiolated GLase-ZZ-His was conjugated to the liposome's surface through the MAL-SH group via a covalent reaction. The immunoliposome was eventually produced through conjugation of the anti-EGFR antibody with the pre-immunoliposome.

3.4. Immunoliposome-mediated delivery of HPTS and imaging of GLase-ZZ-His in U87 ΔEGFR cells

To investigate whether immunoliposomes conjugated with the anti-EGFR antibody targeted U87 ΔEGFR cells and are useful for the delivery of chemicals and the imaging of tumors, HPTS, a fluorescence chemical, was encapsulated in the immunoliposome and U87 ΔEGFR cells were incubated with the HPTS-encapsulated immunoliposomes. Strong bioluminescence was detected in the cells (Fig. 5A). In contrast, pre-immunoliposomes not conjugated to the mAb, emitted a faint signal in the cells (Fig. 5A). Moreover, the cells were subjected to fluorescence microscopy. The fluorescence from HPTS was strong in the immunoliposome-treated cells but weak in the pre-immunoliposome-treated cells (Fig. 5B).

3.5. In vivo imaging of xenografted brain tumor using immunoliposomes conjugated with anti-EGFR antibody

We investigated whether the immunoliposomes conjugated with the anti-EGFR antibody could be used to image xenografted brain tumor and carry chemicals. Immunoliposomes and pre-immunoliposomes were injected into the tail of tumor-bearing mice. After 4 h, the tumor was imaged by injection with 50 μL of coelenterazine solution (100 μg/mL) at the tumor site. A strong and clear bioluminescence signal was detected at the tumor site (Fig. 6A, left panel) in immunoliposome-treated mice while weak signals were detected at two tumor sites in the pre-immunoliposome-treated mice (Fig. 6A, right panel). As a signal intensity control, much weaker signal was observed at the site without tumor when coelenterazine was injected (data not shown).

To investigate whether HPTS was specifically carried in the tumor, the tumor xenografted regions were sectioned and the

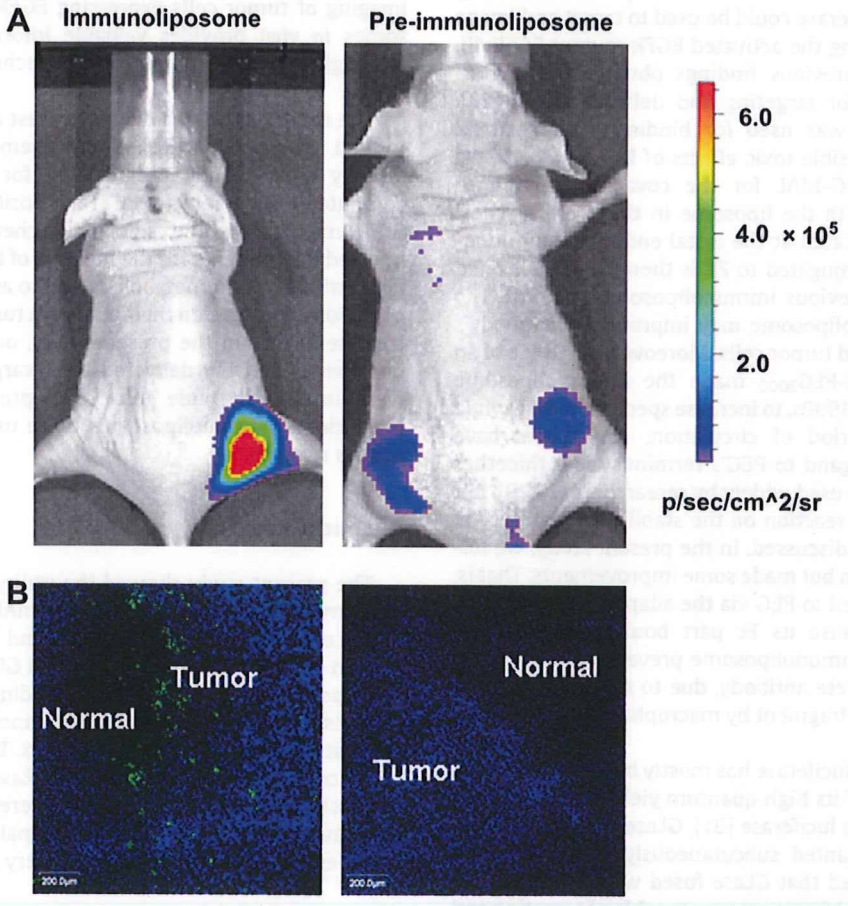

Fig. 6. Bioluminescence imaging in living nude mice harboring U87 ΔEGFR cell xenografts and slice analysis. (A) Images were obtained using a CCD camera 4 h after an intravenous injection of immunoliposomes and pre-immunoliposomes in the tail. A color scale represents p/sec/cm^2/steradian. Left panel, immunoliposome-treated sample. Right panel, pre-immunoliposome-treated sample. (B) A 10-μm section cut from frozen tumor tissue harvested at 4 h post-injection and examined with a confocal microscopy. The tumor section was examined for nuclei stained by Hoechst (blue) and HPTS (green). The blue fluorescence of Hoechst was used to indicate the position of the tumor. Left panel, immunoliposome-treated sample. Right panel, pre-immunoliposome-treated sample. Bar = 200 μm.

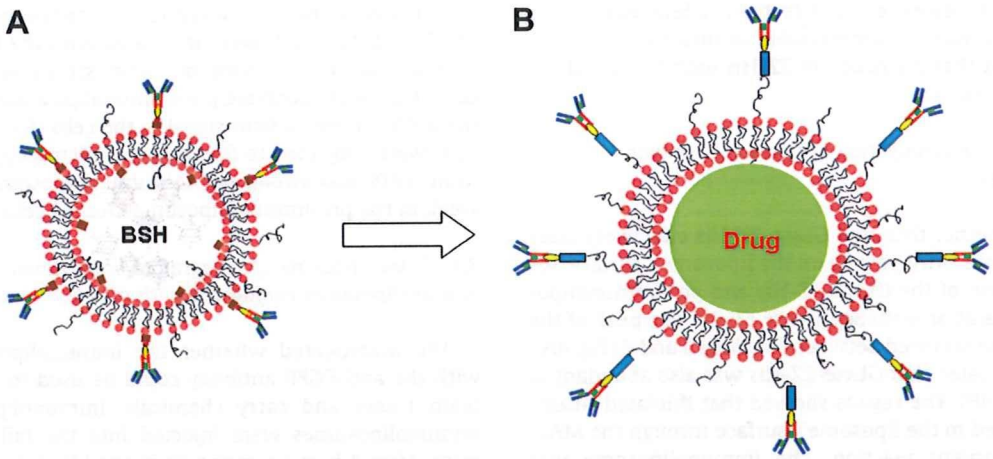

Fig. 7. Development of a bifunctional immunoliposome. (A) Our previous nickel-immunoliposome. (B) The bifunctional immunoliposome.

fluorescence from HPTS was observed using a confocal microscope. The fluorescence was located in the tumor but not in normal tissue in the immunoliposomes-treated mice (Fig. 6B, left panel). In the pre-immunoliposome-treated mice, by contrast, no fluorescence was seen in the tumor or normal regions (Fig. 6B, right panel).

4. Discussion

In the present study, we showed that a fusion protein consisting of ZZ-linked to *Gaussia* luciferase could be used to target and image glioblastoma cells expressing the activated EGFR mutant EGFRvIII. The results support our previous findings obtained with a ZZ conjugated to liposomes for targeting and delivering BSH [23]. Previously, a nickel lipid was used for binding His-tagged ZZ (Fig. 7A) [23]. To avoid possible toxic effects of DOGS-NTA-Ni, we replaced it with DSPE-PEG-MAL for the covalent reaction to conjugate GLase-ZZ-His with the liposome in the present study. Thus, GLase-ZZ-His was located at the distal end of the immunoliposome. The antibody conjugated to ZZ is thought to be located further out than in our previous immunoliposome (Fig. 7B). The design of the new immunoliposome may improve the antibody's ability to recognize and bind tumor cells. Moreover, the usage of an appropriate ratio of DSPE-PEG_{2000} made the immunoliposome more stable. Since the mid-1990s, to increase specific binding while also retaining a long period of circulation, researchers have attached an antibody or ligand to PEG's terminus via a thioether bond [28,29]. This design is used widely by researchers [28,29], but the effect of the thiolation reaction on the stability and affinity of the antibody has not been discussed. In the present study, we followed the same basic design but made some improvements. That is, the antibody was conjugated to PEG via the adaptor GLase-ZZ-His, and remained intact because its Fc part bound with ZZ. The construction of the new immunoliposome prevents shorter circulation times using a complete antibody, due to the rapid identification and uptake of the Fc fragment by macrophages in circulation *in vivo* [30].

In recent years, *Gaussia* luciferase has mostly been used for non-invasive studies because of its high quantum yield compared with firefly luciferase and *Renilla* luciferase [31]. GLase has been used to image cultured cells implanted subcutaneously into nude mice [32]. A recent study showed that GLase fused with an anti-carcinoembryomic antigen (CEA) fragment was capable of targeting and imaging human colon carcinoma cells in nude mice [22]. However, its utilization for detecting the distribution of immunoliposomes has not been reported. In the present study, immunoliposomes conjugated with GLase-ZZ-His and anti-EGFR antibody were used to target and image EGFRvIII-expressing glioma cells both *in vitro* and *in vivo*. Although the luciferase signal was detected at the tumor site by a direct coelenterazine solution injection, the signal intensity is much stronger than those in pre-immunoliposome-treated sample (Fig. 6) and at the site without tumor (data not shown), indicating the GLase on immunoliposome targeted to the tumor site by ZZ conjugated antibody. These results suggest that the bioluminescence of GLase is not affected by thiolation and immunoliposomes conjugated with GLase may be useful for the imaging of tumor cells expressing EGFR. The monitoring of liposomes *in vivo* provides valuable information on drug delivery although the development of this technology is still in its early stages.

The combination of a diagnostic test and a therapeutic entity is termed theranostics [33]. Some chemotherapeutics have been directly or indirectly radiolabeled for single photon emission computed tomography (SPECT) and positron emission tomography (PET) imaging [34]. The radiolabeled chemotherapeutics have been injected into patients for the purpose of better understanding their biodistribution and metabolism and to assess whether there exists a relationship between their uptake in tumor tissue and response to treatment [34]. In the present study, our bifunctional immunoliposomes effectively delivered their cargo to the tumor and also were imaged in nude mice. The present results suggest our bifunctional immunoliposomes to be useful for BNCT as a theranostics reagent.

5. Conclusions

The present study showed the utility of bifunctional immunoliposomes fused with GLase-ZZ-His-mAb for the imaging and targeting of glioma cells both *in vitro* and *in vivo*. A thiolated fusion protein of ZZ (Fc-affinity domain) and GLase was conjugated to the immunoliposomes for antibody binding and imaging. We have demonstrated the utility of *Gaussia princeps* luciferase for detecting the distribution of immunoliposomes. Bioluminescence and fluorescence analyses indicated that GLase-ZZ-His and HPTS were successfully delivered into EGFR-overexpressing glioma cells *in vitro* and *in vivo*. Thus, our bifunctional immunoliposome system provides the potential for drug delivery and imaging in tumors.

Acknowledgements

This work was supported by a Grant-in-aid for Scientific Research from the Ministry of Education, Science, Sports and

Culture of Japan and by a Grant-in-aid for Scientific Research from the Ministry of Health, Labour and Welfare of Japan.

Supplementary data

Supplementary material associated with this paper can be found, in the online version, at doi:10.1016/j.biomaterials.2010.01.086

Appendix

Figures with essential colour discrimination. Certain figures in this article, in particular Figs. 4 and 7, that are difficult to interpret in black and white. The full colour images can be found in the online version, at doi:10.1016/j.biomaterials.2010.01.086

References

[1] Maurer N, Fenske DB, Cullis PR. Developments in liposomal drug delivery systems. Expert Opin Biol Ther 2001;1:923–47.
[2] Jiang W, Kim BY, Rutka JT, Chan WC. Advances and challenges of nanotechnology-based drug delivery systems. Expert Opin Drug Deliv 2007;4:621–33.
[3] Elbayoumi TA, Pabba S, Roby A, Torchilin VP. Antinucleosome antibody-modified liposomes and lipid-core micelles for tumor-targeted delivery of therapeutic and diagnostic agents. J Liposome Res 2007;17:1–14.
[4] Sajja HK, East MP, Mao H, Wang YA, Nie S, Yang L. Development of multifunctional nanoparticles for targeted drug delivery and noninvasive imaging of therapeutic effect. Curr Drug Discov Technol 2009;6:43–51.
[5] Pan XQ, Wang H, Lee RJ. Boron delivery to a murine lung carcinoma using folate receptor-targeted liposomes. Anticancer Res 2002;22:1629–33.
[6] Maruyama K, Ishida O, Kasaoka S, Takizawa T, Utoguchi N, Shinohara A, et al. Intracellular targeting of sodium mercaptoundecahydrododecaborate (BSH) to solid tumors by transferrin-PEG liposomes, for boron neutron-capture therapy (BNCT). J Control Release 2004;98:195–207.
[7] Bohl Kullberg E, Bergstrand N, Carlsson J, Edwards K, Johnsson M, Sjöberg S, et al. Development of EGF-conjugated liposomes for targeted delivery of boronated DNA binding agents. Bioconjug Chem 2002;13:737–43.
[8] Sofou S, Sgouros G. Antibody-targeted liposomes in cancer therapy and imaging. Expert Opin Drug Deliv 2008;5:189–204.
[9] Erdogan S, Roby A, Sawant R, Hurley J, Torchilin VP. Gadolinium-loaded polychelating polymer-containing cancer cell-specific immunoliposomes. J Liposome Res 2006;16:45–55.
[10] Kostarelos K, Emfietzoglou D. Tissue dosimetry of liposome-radionuclide complexes for internal radiotherapy: toward liposome-targeted therapeutic radiopharmaceuticals. Anticancer Res 2000;20:3339–45.
[11] Erdogan S, Medarova ZO, Roby A, Moore A, Torchilin VP. Enhanced tumor MR imaging with gadolinium-loaded polychelating polymer-containing tumor-targeted liposomes. J Magn Reson Imaging 2008;27:574–80.
[12] Torchilin VP. Polymeric contrast agents for medical imaging. Curr Pharm Biotechnol 2000;1:183–215.
[13] Weng KC, Noble CO, Papahadjopoulos-Sternberg B, Chen FF, Drummond DC, Kirpotin DB, et al. Targeted tumor cell internalization and imaging of multifunctional quantum dot-conjugated immunoliposomes *in vitro* and *in vivo*. Nano Lett 2008;8:2851–7.
[14] Welsh DK, Kay SA. Bioluminescence imaging in living organisms. Curr Opin Biotechnol 2005;16:73–8.
[15] Swijnenburg RJ, Schrepfer S, Cao F, Pearl JI, Xie X, Connolly AJ, et al. *In vivo* imaging of embryonic stem cells reveals patterns of survival and immune rejection following transplantation. Stem Cells Dev 2008;17:1023–9.
[16] Bhaumik S, Lewis XZ, Gambhir SS. Optical imaging of Renilla luciferase, synthetic Renilla luciferase, and firefly luciferase reporter gene expression in living mice. J Biomed Opt 2004;9:578–86.
[17] Thompson EM, Adenot P, Tsuji FI, Renard JP. Real time imaging of transcriptional activity in live mouse preimplantation embryos using a secreted luciferase. Proc Natl Acad Sci U S A 1995;92:1317–21.
[18] Verhaegent M, Christopoulos TK. Recombinant *Gaussia* luciferase. Overexpression, purification, and analytical application of a bioluminescent reporter for DNA hybridization. Anal Chem 2002;74:4378–85.
[19] Tannous BA. *Gaussia* luciferase reporter assay for monitoring biological processes in culture and *in vivo*. Nat Protoc 2009;4:582–91.
[20] Suzuki T, Usuda S, Ichinose H, Inouye S. Real bioluminescence imaging of a protein secretory pathway in living mammalian cells using *Gaussia* luciferase. FEBS Lett 2007;581:4551–6.
[21] Venisnik KM, Olafsen T, Loening AM, Iyer M, Gambhir SS, Wu AM. Bifunctional antibody-Renilla luciferase fusion protein for *in vivo* optical detection of tumors. Protein Eng Des Sel 2006;19:453–60.
[22] Venisnik KM, Olafsen T, Gambhir SS, Wu AM. Fusion of *Gaussia* luciferase to an engineered anti-carcinoembryonic antigen (CEA) antibody for *in vivo* optical imaging. Mol Imaging Biol 2007;9:267–77.
[23] Feng B, Tomizawa K, Michiue H, Miyatake S, Han XJ, Fujimura A, et al. Delivery of sodium borocaptate to glioma cells using immunoliposome conjugated with anti-EGFR antibodies by ZZ-His. Biomaterials 2009;30:1746–55.
[24] Feng B, Zhao CH, Tanaka S, Imanaka H, Imamura K, Nakanishi K. TPR domain of Ser/Thr phosphatase of *Aspergillus oryzae* shows no auto-inhibitory effect on the dephosphorylation activity. Int J Biol Macromol 2007;41:281–5.
[25] Hashizume T, Fukuda T, Nagaoka T, Tada H, Yamada H, Watanabe K, et al. Cell type dependent endocytic internalization of ErbB2 with an artificial peptide ligand that binds to ErbB2. Cell Biol Int 2008;32:814–26.
[26] Tomizawa K, Iga N, Lu YF, Moriwaki A, Matsushita M, Li ST, et al. Oxytocin improves long-lasting spatial memory during motherhood through MAP kinase cascade. Nat Neurosci 2003;6:384–90.
[27] Kheirolomoom A, Ferrara KW. Cholesterol transport from liposomal delivery vehicles. Biomaterials 2007;28:4311–20.
[28] Béduneau A, Saulnier P, Hindré F, Clavreul A, Leroux JC, Benoit JP. Design of targeted lipid nanocapsules by conjugation of whole antibodies and antibody Fab' fragments. Biomaterials 2007;28:4978–90.
[29] Kirpotin D, Park JW, Hong K, Zalipsky S, Li WL, Carter P, et al. Sterically stabilized anti-HER2 immunoliposomes: design and targeting to human breast cancer cells in vitro. Biochemistry 1997;36:66–75.
[30] Kamps JA, Scherphof GL. Receptor versus non-receptor mediated clearance of liposome. Adv Drug Deliv Rev 1998;32:81–97.
[31] Tannous BA, Kim DE, Fernandez JL, Weissleder R, Breakefield XO. Codon-optimized *Gaussia* luciferase cDNA for mammalian gene expression in culture and *in vivo*. Mol Ther 2005;11:435–43.
[32] Wurdinger T, Badr C, Pike L, de Kleine R, Weissleder R, Breakefield XO, et al. A secreted luciferase for *ex vivo* monitoring of *in vivo* processes. Nat Methods 2008;5:171–3.
[33] Del Vecchio S, Zannetti A, Fonti R, Pace L, Salvatore M. Nuclear imaging in cancer theranostics. Q J Nucl Med Mol Imaging 2007;51:152–63.
[34] Rottey S, Signore A, Van de Wiele C. Radiolabelled chemotherapeutics. Q J Nucl Med Mol Imaging 2007;51:139–51.

初発膠芽腫に対するホウ素中性子捕捉療法、X線追加照射、化学療法の多施設第II相臨床試験

試験実施計画書

主任研究者　　大阪医科大学　脳神経外科　　宮武　伸一

副主任研究者　　京都大学原子炉実験所　附属粒子線腫瘍学研究センター
小野　公二

2009年　6月　29日　財）　臨床研究情報センター倫理委員会承認（第2版）

秘密保持に関する供述：

本試験実施計画書は、本試験に直接係わる者及び倫理審査委員会以外の者に情報を開示してはならない。また、本情報は事前の書面による宮武伸一の承諾なしに本試験の実施あるいは評価以外の目的に利用してはならない。

本試験に関与するすべての者は「世界医師会ヘルシンキ宣言」および「臨床研究に関する倫理指針」に従う。

略語一覧

略語	語形	
ACNU	1-(4-amino-2-methyl-5-pyrimidynyl) methyl-3-(2-chloroethyl)-3-nitrosourea hydrochloride	ニムスチン
ADR	adverse drug reaction	薬物有害反応
AE	adverse event	有害事象
AUC	area under the blood concentration time curve	時間曲線下面積
BNCT	boron neutron capture therapy	ホウ素中性子捕捉療法
BPA	p-boronophenylalanine	パラボロノフェニールアラニン
BSH	sodium borocaptate	ボロカプテイト
CBE	compound biological effectiveness	化合物の微視的集積パターンに依存する生物学的効果比
CNS	central nervous system	全原発性中枢神経系
CTC	common terminology criteria for adverse events	有害事象 共通毒性規準
CTV	clinical target volume	臨床標的体積
DDW	distilled water	蒸留水
EORTC	European organisation for research and treatment of cancer	欧州癌研究治療機構
F-BPA-PET	fluoride-labeled boronophenylalanine-PET	fluoride-labeled boronophenylalanine を用いた PET
GMP	Good Manufacturing Practice	医薬品及び医薬部外品の製造管理及び品質管理の基準
GTV	gross tumor volume	総腫瘍量
ICMJE	International Committee of Medical Journal Editors	医学雑誌編集者国際委員会
ICP	Inductively Coupled Plasma	誘導結合プラズマ
IFN	interferon	インターフェロン
JCDS	Jaeri Computational Dosimetry System	-
JCOG	Japan Clinical Oncology Group	日本臨床腫瘍研究グループ
JRR4	Japan Research Reactor No. 4	日本原子力研究開発機構国産 4 号炉
KPS	Karnofsky Performance Scale	-
L/N 比	Lesion/Normal ratio	病変/正常脳比
KUR	Kyoto university reactor	京都大学研究炉
MDS	myelodysplastic syndrome	骨髄異型性症候群

MGMT	methylguanine-DNA methyltransferase	-
MTIC	5- [(1*Z*) -3-Methyltriaz-1-en-1-yl] -1*H*-imidazole-4-carboxamide	-
NCIC	National cancer institute of canada	カナダ国立がん研究所
NYHA	New York Heart Association	ニューヨーク心臓協会
PET	positron emission tomography	ポジトロン・エミッション・トモグラフィー
RBE	relative biological effectiveness	生物学的効果比
RPA	Recursive Partitioning Analysis	予後因子別分類
SAE	serious adverse event	重篤な有害事象
SERA	Simulation Environment for Radiotherapy Applications	-
tmax	maximum drug concentration time	最高血中濃度到達時間
TMZ	temozolomide	テモゾロマイド
TRI	Translational Research Informatics Center	臨床研究情報センター
VEGF	vascular endothelial growth factor	血管内皮細胞増殖因子
WHO	world health organization	世界保健機構
XRT	X-ray radiation treatment	X線照射治療

目次

0. 概要 1
0.1 シェーマ 1
0.2 目的 2
0.3 主な適格規準 2
0.4 目標症例数 2
0.5 試験デザイン 2
0.6 連絡先 3
1. 目的 4
2. 背景と根拠 4
3. 薬物情報および X 線照射情報 6
3.1 X 線照射 6
4. 診断基準と病期・病型分類 14
4.1. 診断基準 14
4.2. 病期分類 14
5. 適格規準 14
5.1 選択規準 14
5.2 除外規準 15
6. 説明と同意 15
7. 登録 16
7.1 倫理審査委員会の承認 16
7.2 登録の手順 16
8. 治療計画 17
8.1 プロトコル治療 17
8.2 プロトコル治療中止規準 24
8.3 併用療法 24
9. 有害事象の評価・報告 25
9.1 有害事象の定義 25
9.2 adverse drug reaction (ADR: adverse drug reaction) 25
9.3 予測できない薬物有害反応 (unexpected adverse drug reaction) 25
9.4 有害事象の評価と報告 25
10. 観察・検査・報告項目とスケジュール 32
10.1 観察・検査項目および報告すべき治療情報 32
10.2 観察・検査・報告スケジュール 35
11. 目標症例数と試験期間 36
11.1 目標症例数 36
11.2 試験期間 36
12. エンドポイントの定義 36

12.1. 主要評価項目 36
12.2. 副次評価項目 36
13. 統計学的考察 39
13.1 目標症例数の設定根拠 39
13.2 解析対象集団 39
13.3 解析項目・方法 39
14. 症例報告書の記入と提出 40
14.1 様式と提出期限 40
14.2 紙症例報告書の記入方法 41
14.3 症例報告書内容の確認と問い合わせ 41
15. モニタリング 42
15.1 進捗管理 42
16. 各種委員会 42
16.1 独立データモニタリング委員会 42
16.2 中央病理判定委員会 43
16.3 中央効果判定委員会 43
17. 倫理的事項 43
17.1 遵守すべき諸規則 43
17.2 説明文書・同意書（様式）の作成と改訂 43
17.3 個人情報の保護 45
18. 試験の費用負担 45
18.1 資金源および財政上の関係 45
18.2 試験治療に関する費用 45
18.3 健康被害に対する補償 45
19. プロトコルの改訂 45
20. 試験の終了と早期中止 46
20.1 試験の終了 46
20.2 試験の早期中止 46
21. 記録の保存 47
22. 研究結果の帰属と公表 48
23. 研究組織 48
23.1 主任研究者 48
23.2 副主任研究者 48
23.3 研究事務局および担当者 48
23.4 プロトコル作成者 48
23.5 統計解析責任者 48
23.6 データセンター 49
23.7 独立データモニタリング委員 49

23.8 中央病理判定委員会 49
23.9 中央効果判定委員会委員 49
23.10 試験参加予定施設および試験責任医師 49
24. 文献 49
25. 付録 51
付録 1. Karnofsky performance scale 52
付禄 2. New York Heart Association (NYHA)の心機能分類 53
付録 3. NCI-CTC AE Ver3.0 日本語版 54
付録 4. 薬剤添付情報 55
付録 5. 施設登録依頼書 61
付録 6. 症例登録票 62
付録 7. 匿名化番号対照表 63
付録 8. 重篤な有害事象発生時の報告・対応マニュアル 65
付録 9. 説明・同意文書　(見本) 70

0. 概要

0.1 シェーマ

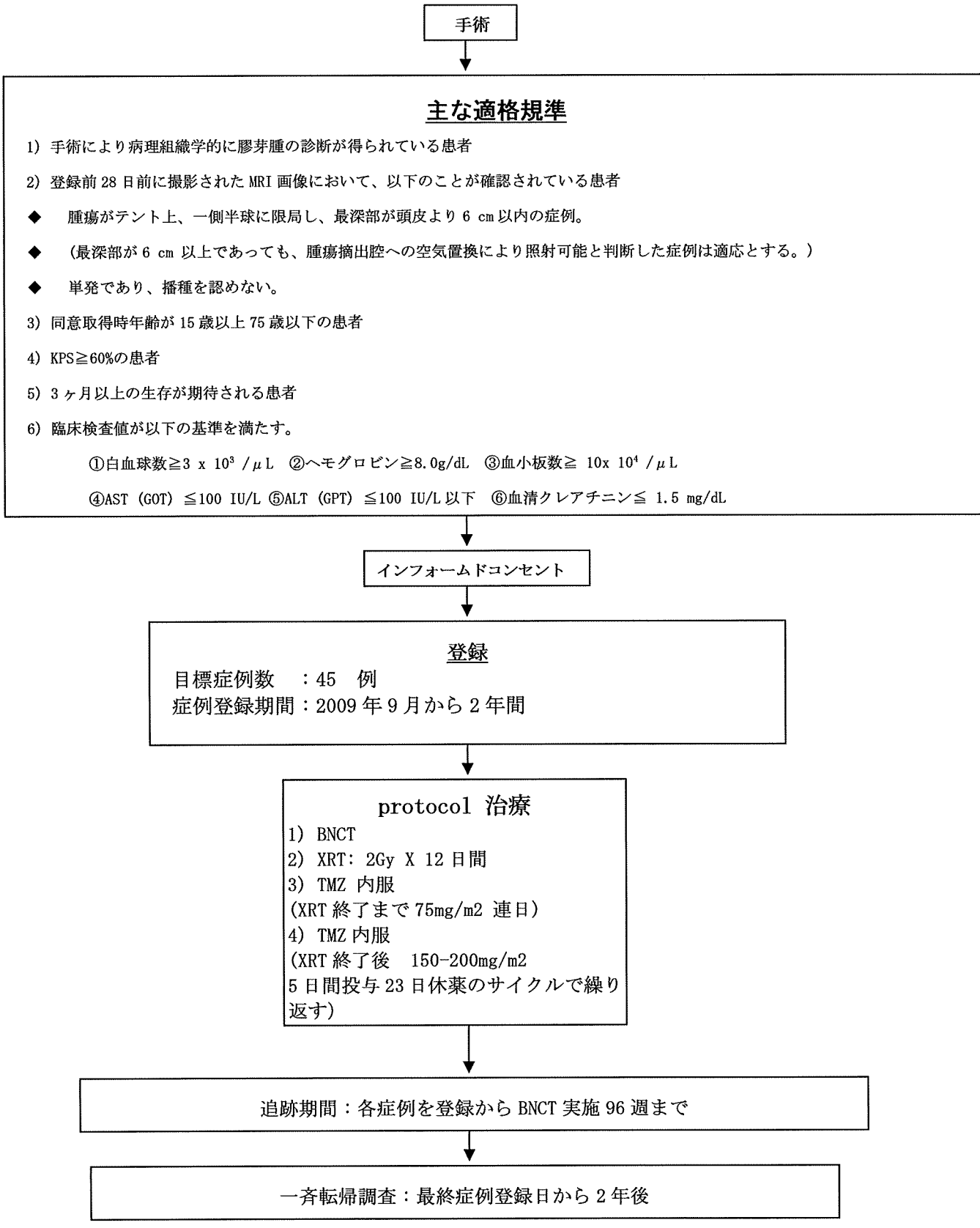
手術
主な適格規準
1) 手術により病理組織学的に膠芽腫の診断が得られている患者
2) 登録前 28 日前に撮影された MRI 画像において、以下のことが確認されている患者
◆ 腫瘍がテント上、一側半球に限局し、最深部が頭皮より 6 cm 以内の症例。
◆ (最深部が 6 cm 以上であっても、腫瘍摘出腔への空気置換により照射可能と判断した症例は適応とする。)
◆ 単発であり、播種を認めない。
3) 同意取得時年齢が 15 歳以上 75 歳以下の患者
4) KPS≧60%の患者
5) 3 ヶ月以上の生存が期待される患者
6) 臨床検査値が以下の基準を満たす。
①白血球数≧3 x 10^3 /μL ②ヘモグロビン≧8.0g/dL ③血小板数≧ 10x 10^4 /μL
④AST (GOT) ≦100 IU/L ⑤ALT (GPT) ≦100 IU/L 以下 ⑥血清クレアチニン≦ 1.5 mg/dL
インフォームドコンセント
登録
目標症例数 ：45 例
症例登録期間：2009 年 9 月から 2 年間
protocol 治療
1) BNCT
2) XRT: 2Gy X 12 日間
3) TMZ 内服
(XRT 終了まで 75mg/m2 連日)
4) TMZ 内服
(XRT 終了後 150-200mg/m2
5 日間投与 23 日休薬のサイクルで繰り返す)
追跡期間：各症例を登録から BNCT 実施 96 週まで
一斉転帰調査：最終症例登録日から 2 年後

0.2 目的

初発膠芽腫を対象として、主要評価項目を全生存期間(overall survival)、副次評価項目を腫瘍縮小効果(tumor response)と有害事象の発現とし、ホウ素中性子捕捉療法 (boron neutron capture therapy, BNCT) 及び 24GyX 線分割外照射(XRT)後に Temozolomide (TMZ) を併用した放射線化学療法の治療効果を検討する。

0.3 主な適格規準

1) 手術により病理組織学的に膠芽腫の診断が得られている患者
2) 手術前 28 日前に撮影された MRI 画像において、以下のことが確認されている患者
◆ 腫瘍がテント上、一側半球に限局し、最深部が頭皮より 6 cm 以内の症例。(最深部が 6 cm 以上であっても、腫瘍摘出腔への空気置換により照射可能と判断した症例は適応とする。)
◆ 単発であり、播種を認めない。
3) 同意取得時年齢が 15 歳以上 75 歳以下の患者 (但し、満 15 歳以上 19 歳以下の場合は、試験参加について患者本人および代諾者から文面で同意が得られている。)
4) Karnofsky Performance Scale (KPS) が 60%以上の患者
5) 3 ヶ月以上の生存が期待される患者
6) 手術後かつ登録前 28 日以内の臨床検査において、主要臓器の機能が十分に保持されており、以下の条件を満たす患者

白血球数	3,000 /μL 以上
ヘモグロビン	8.0g/dL 以上 (登録前 28 日以内までに輸血を行っていないこと)
血小板数	100,000 /μL 以上
AST (GOT)	100 IU/L 以下
ALT (GPT)	100 IU/L 以下
血清クレアチニン	1.5 mg/dL 以下

7) 本試験への参加について本人の同意が文書で得られている患者

但し 説明内容の理解・同意が可能であっても神経症状によって患者本人の署名が困難である場合、患者本人の同意の確認の署名を代筆者が行っても良い。

0.4 目標症例数

目標症例数： 45 例
症例登録期間 ： 2009 年 9 月 1 日～2011 年 8 月 31 日
追跡終了日 ： 最終症例登録日から 2 年後

0.5 試験デザイン

試験の相 ：第 II 相
試験のデザイン ：単一群試験
対照の種類 ：無